Lasers in Manufacturing Conference 2023

Advanced laser irradiation strategies for tailoring temperature profiles for laser-based powder bed fusion (PBF-LB/P) of highly absorbing polymers

Vadim Medvedev[a,b,c,*] , Sebastian-Paul Kopp [a,b,c], Stephan Roth[a,b,c]

[a] *Bayerisches Laserzentrum GmbH, Konrad-Zuse-Straße 2-6, 91052 Erlangen, Germany*
[b]*Collaborative Research Center (CRC) 814 "Additive Manufacturing", Am Weichselgarten 10, 91058 Erlangen-Tennenlohe, Germany*
[c]*Erlangen Graduate School in Advanced Optical Technologies (SAOT), Paul-Gordan-Straße 6, 91052 Erlangen, Germany*

Abstract

Additively manufactured parts consisting of polymer powders blended with carbon black have increased protection against ultraviolet radiation and thus are beneficial for applications involving intensive exposure to sunlight. However, this powder blends are challenging to be processed in laser-based powder bed fusion of polymers (PBF-LB/P) due to their high absorptivity of infrared radiation. Thus, precisely tailoring the energy input provided by a CO_2-laser is crucial for enhancing process stability for processing highly absorptive polymers. Adapting the laser energy input by applying advanced irradiation strategies offers the possibility to tailor the temperature profiles during PBF-LB/P process. In this study, the effect of advanced laser irradiation strategies with pixel-encoded energy densities on the adaption of the temperature profile of polymer powders blended with carbon black is investigated. Finally, irradiation patterns are defined to achieve spatially tailored temperature profiles across the powder layer for demonstration the capabilities of the developed scanning strategy.

Keywords: Laser powder bed fusion; laser illumination strategy; carbon black; temperature profile; selective laser sintering

1. Introduction

Laser-based powder bed fusion (PBF-LB), compared to other additive manufacturing (AM) technologies, offers the significant advantage of a diverse choice of materials, including polymers, metals, ceramics, and composites (Han et al., 2022). Composites include polymer-metal, polymer-polymer, polymer-ceramic, and purely ceramic materials (Diegel et al., 2019; Kruth et al., 2003). Currently, polymers and metals are commonly used and popular materials for PBF-LB (Leary, 2020). PBF-LB/P has the additional advantage that sintered parts have mechanical properties comparable to those of solid components fabricated by injection molding or casting, mainly because of the powerful interfacial adhesion of the layers created during sintering (Athreya et al., 2011a; Van Hooreweder et al., 2013; Zhu et al., 2015).

Some studies have focused on the addition of reinforcing materials to improve various characteristics of sintered plastic parts (Caulfield et al., 2007; Ho et al., 1999; Shi et al., 2008). They have reported on the effective enhancement of thermal and electrical properties of sintered parts by incorporating fillers into neat PA12. These fillers include nano-sized carbon black (Athreya et al., 2010, 2011b), carbon fiber (Yan et al., 2011), and other electrically or thermally conducting materials (Fantino et al., 2018; Li et al., 2017). For many years, carbon black has served as a recognized light-stabilizing additive in different polymers. It is thought to act as a basic physical screen, an UV absorber and a terminator of free radical chains, which propagate photo-oxidative reactions (Hawkins, W. L., 1960, 1963). Therefore, it is important to be able to sinter the powder blends containing additives in the form of carbon black in the PBF-LB/P process.

However, the presence of carbon black particles in base polymer powder increases CO_2 laser radiation absorption during sintering as carbon black acts as an infrared absorbing additive (Wagner et al., 2004), which can lead to local overheating and an increase of thermal stresses in the sintered layer during PBF-LB/P process. Therefore, creating a composite blend containing carbon black and polymer particles changes the behavior of the temperature profile during sintering of the powder mixture and cause sintering inconsistencies and leading to defects such as cracking, warping and delamination (Rong-ji et al., 2009; Singh et al., 2012).

The authors (John D williams & Carl R. Deckard, 1998; Manshoori Yeganeh et al., 2019; Shen et al., 2021) showed that the use of a conventional meander scanning strategy and constant laser energy density (power, scanning speed and hatch distance are constant) during sintering of the powder layer leads to non-uniform temperature distribution, which in turn reduces the quality of the part due to the presence of different thermal stress in different areas of the part. Especially during processing of powder mixtures with higher infrared absorptivity the inhomogeneity of the temperature distribution will be more pronounced. Hence, it is imperative to develop a laser energy density control method to effectively minimize temperature deviations across various regions during sintering a single powder layer.

With the increasing complexity of products, the need for parts consisting of multi-materials is becoming more and more important in industry. Therefore, for the simultaneous sintering of different powders with different melting temperatures it is necessary to be able to tailor the laser energy density and accordingly the temperature profiles. The authors (Laumer et al., 2014) used two laser sources to create a part consisting of multiple materials. The first laser additionally distributed the required preheating temperature of the higher-melting polymer, and the second laser distributed the energy required to melt the two preheated powders simultaneously. This approach is complex and resource-intensive because it requires two laser sources.

The presented work, for the first time, will investigate laser irradiation strategy with the possibility of manipulating the energy density during sintering of a single powder layer. To determine the suitability of the investigated scanning strategy in the PBF-LB/P process, the temperature profiles and densities of the sintered layers generated by the developed scanning strategy will be compared with the well-established scanning strategy for powder sintering process. Finally, the capabilities of the developed scanning strategy in terms of creating and tailoring arbitrary temperature profiles or in other words tuning the laser energy density within a single layer will be demonstrated on a polymer powder mixed with carbon black.

2. Materials and Methods

2.1. Experimental setup

The decisive parts of the experimental setup are the building chamber of the setup for laser-based powder bed fusion of polymers (PBF-LB/P) (Stichel et al., 2020), the adjustable film applicator, the laser source and the infrared camera. The powder layer was prepared using an adjustable film applicator (Thierry GmbH, Stuttgart, Germany) similar to the doctor blade applicators which are used in PBF-LB/P process (see Fig. 1). The adjustable film applicator allowed to precisely control the thickness of the powder layer, which is critical for the experimental investigations. A uniform layer of powder was evenly spread on the building platform, ensuring a consistent thickness of 400 µm using the film applicator. Such layer thickness imitates the first layer in the PBF-LB/P process because the first layer is always thicker than the subsequent layers, which are typically 100-150 µm (Han et al., 2022).

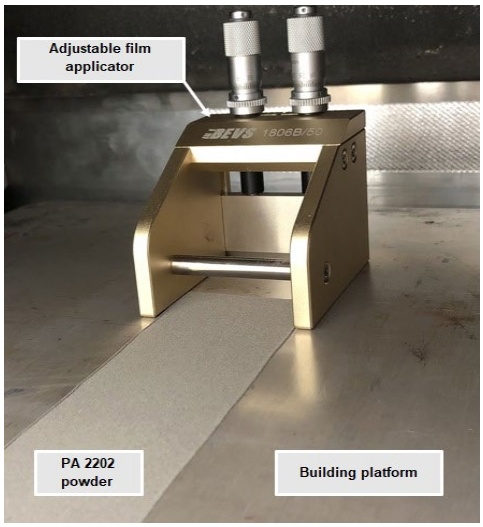

Fig. 1. Preparation of the powder layer on the building platform with an adjustable film applicator

The equipment for sintering powder layer consisted of a CO_2-Laser with a maximum output power of 60 W (Synrad ti60, Novanta Photonics, Seattle, WA, USA) and a laser scanner (Miniscan II-20, Raylase GmbH, Weßling, Germany) as well as a F-Theta lens with a focal length = 420 mm (Raylase GmbH, Weßling, Germany). During the sintering process, the temperature was monitored using an infrared camera (Millenium 1310k SM PRO, IRCAM GmbH, Erlangen, Germany). The infrared camera provided non-contact temperature measurements, allowing for real-time monitoring of the temperature profiles across the powder layer during the sintering process. Experimental investigations in this paper were carried out using black pigment-filled polyamide 12 powder (PA2202, EOS GmbH, Krailling, Germany).

2.2. Creation of pixel-encoded scanning strategies (PESS)

WeldMARK 3.0 software (Raylase GmbH, Weßling, Germany) was used to create scanning strategies for sintering the powder layer. First and foremost, the meander scanning strategy (MSS) was created by well-established vector approach for PBF-LB/P (Han et al., 2022; RaylaseAG, 2014). In this case, the laser beam

follows a meandering pattern moving the beam back and forth along parallel scanning lines separated by hatch distance across the powder layer to selectively fuse the particles together (Han et al., 2022). Thus, the energy density applied to the powder layer remains constant, since the laser power, scanning speed and hatch distance remain unchanged during irradiation process.

However, weldMARK 3.0 software also allows to mark bitmap objects, which are rectangular groups of pixels. Thus, bitmap approach makes it possible to integrate bitmap images such as logos or custom graphics into the marking process. In contrast to the vector approach, the laser beam irradiates the surface pixel by pixel based on the bitmap image's matrix. The laser energy density is modulated according to the intensity value of each pixel in the bitmap image during laser marking process (RaylaseAG, 2014). In this work, grayscale image will be used as a scanning strategy for sintering a powder layer in the PBF-LB/P process. The advantage of such pixel-encoded scanning strategy (PESS) is the possibility to tailor the energy density during the sintering of a single powder layer. In this way, the energy density can be encoded into the 256 shades (values) of gray pixels that make up the grayscale image. Each shade of gray pixel represents the intensity value of that pixel.

In the case of MSS, parameters as the shape and size of the sample´s cross section (created by vector approach), laser power, scanning speed and hatch distance are mandatory. While in the case of PESS, additional parameters are added, such as the size of the sample´s cross section in pixels (created by bitmap approach), intensity value of pixels, dots per inch (dpi), maximum pixel exposure time ($t_{\max PE}$) and minimum pixel exposure time ($t_{\min PE}$) (see Table 1). In case PESS, the hatch distance is determined by adjusting the parameters, encompassing the size of the sample's cross-section in pixels and dpi and was set to 0,15 mm.

Table 1. Parameters of investigated scanning strategies

	Power, *W*	Scanning speed, $^{mm}/_{s}$	Hatch distance, *mm*	Shape	Size, *mm*	Size in pixels	dpi	$t_{\max \mathrm{PE}}$, *µs*	$t_{\min \mathrm{PE}}$, *µs*
MSS	5,1	85	0,15	Square	15x15	-	-	-	-
PESS0	5,1	-	-	Square	15x15	38x38	171	1500	0
PESS1	5,1	-	-	Square	15x15	38x38	171	1250	250
PESS2	5,1	-	-	Square	15x15	38x38	171	1250	250

The key parameters in case of PESS are the intensity value of pixels, $t_{\max PE}$ and $t_{\min PE}$, which in turn replace the use of the scanning speed parameter in the case of MSS. For example, if the grayscale image consists of pixels with three intensity values (0 - black pixel, 128 - gray pixel and 255 - white pixel) and the time parameters $t_{\max \mathrm{PE}}$ = 2000 µs, $t_{\min \mathrm{PE}}$ = 1000 µs are used, then the black pixel will be exposed to laser radiation for 2000 µs, the gray pixel for 1500 µs and the white pixel for 1000 µs, while keeping the laser power constant. Therefore, by using PESS it was possible to tailor the temperature profile in the limits of the sintering of a single powder layer. In the presented work, four scanning patterns (see Fig. 2) were investigated.

Fig. 2. Investigated scanning patterns; a) MSS; b) PESS0 (all pixels are black [intensity value = 0]); c) PESS1 (half of the pixels are black [intensity value = 0] and half of the pixels are gray [intensity value = 48]); d) PESS2 (pixels in the central region are black [intensity value = 0] and pixels in the side regions are gray [intensity value = 48])

2.3. Measurement of temperature profile of single powder layers

The measurement of the temperature profile of sintering powder layers was carried out using IRCAM Works software (IRCAM GmbH, Erlangen, Germany) with data recording frame rate per second f_{rec} = 100 fps. The thermal imaging system allowed determining the temperature profiles in the x-y plane of the powder layer. The melting temperature of the PA 2202 powder is specified by the powder manufacturer as 176 °C. Based on this data, the integration time (t_{int}) was set to 50 µs, since according to the specifications of the infrared camera manufacturer, this integration time is necessary for correct measurement of temperatures in the range from 50 °C to 175 °C. Figure 3 illustrates IRCAM Works software interface with a template for measuring the temperature profiles (in five measuring points) of sintering powder for defined scanning strategies.

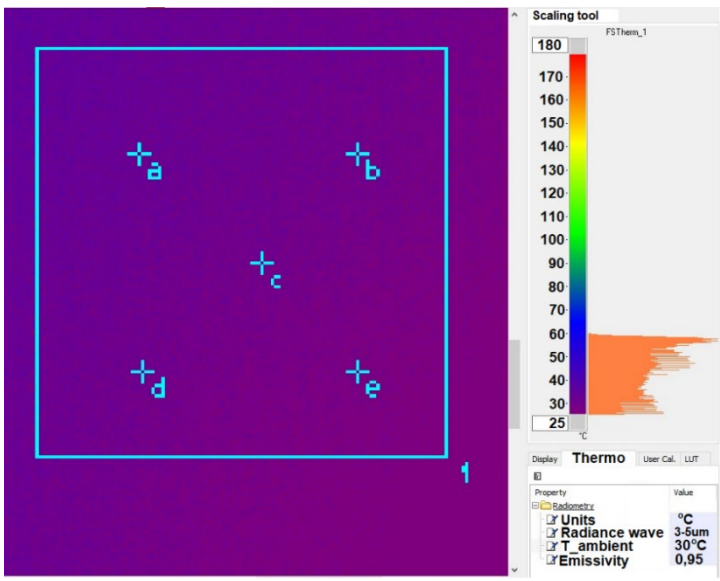

Fig. 3. IRCAM Works software for measuring temperature profiles

The room temperature during the experiments was 30 °C. In order to measure the temperature of the PA 2202 powder during laser sintering, the emissivity set for measuring the surface temperature of powder layer was adjusted to 0.95 (Wegner, 2015). During the sintering process of the powder layer, the software recorded temperature and time data at five defined measuring points (see Fig. 3) for further analysis. The square contour corresponds to the sintering area of the powder bed.

2.4. Analysis of sintered layers structure

Images of the sintered layers were taken with a camera (Iphone 8 Plus, Apple Inc., CA, USA) with a resolution of 4032 x 3024 pixels. In order to evaluate the structure of sintered powder layers irradiated with different scanning strategies an image processing program (ImageJ, National Institutes of Health, Bethesda, MD, USA) was used. By converting a color image into an 8-bit image and applying the triangle thresholding method (Papadopulos et al., 2009) to convert the 8-bit image into a binary image, it was possible to quantify the density of the sintered layers. The ratio of black (sintered regions) and white (un-sintered regions) pixels in three equally distributed rectangular areas within the sintered layers, yielded the corresponding mean density of the sintered layer as well as standard deviation.

3. Results and Discussion

3.1. Temperature profile comparison of MSS and PESS

To evaluate the effect of different scanning strategies on the temperature profile during powder sintering, two distinct scanning strategies (MSS and PESS) were compared. The purpose of this investigation was to determine the PESS and its parameters in order to achieve a similar temperature profile to the MSS. The similarity of the temperature profiles proves that PESS is also applicable to the PBF-LB/P process and allows further adaptation of the temperature profiles during sintering of the powder bed. Powder preheating was not required during the experiments because only single layers were investigated. Figure 4 illustrates the temperature profiles measured at five points for MSS and PESS0 (cf. parameters of scanning strategies in Table 1). Remarkably, despite their differences, both scanning strategies resulted in identical temperature profiles, indicating similar thermal behavior of the powder layer throughout the sintering process.

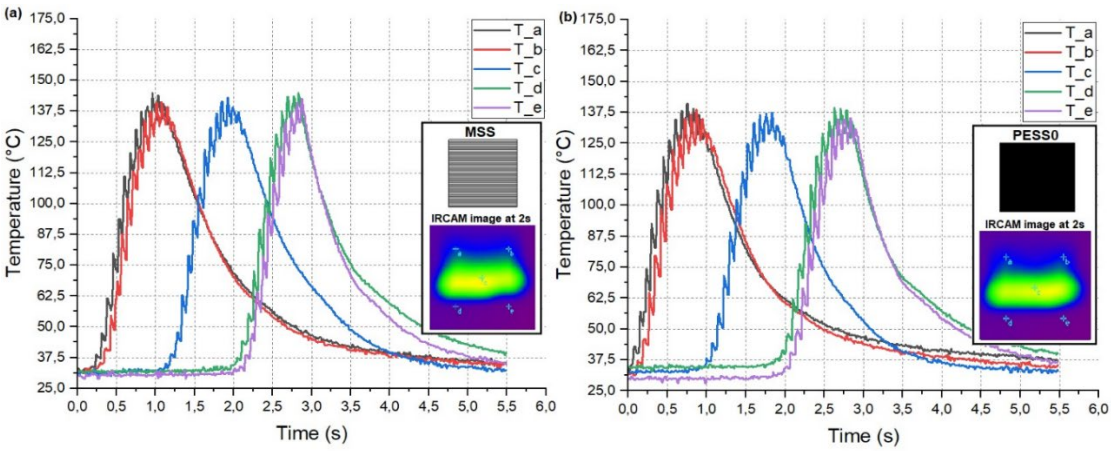

Fig. 4. Temperature profiles caused by different scanning strategies measured at five points; a) MSS; b) PESS0

For MSS, the temperature profile of measuring point 'd' experiences the highest peak temperature, reaching a value of 144.84 °C. On the other hand, among temperature profiles of five measuring points, point 'a' exhibits the lowest peak temperature, measuring at 141.11 °C. For PESS0, the temperature profile of measurement point 'a' has the highest temperature (140.98°C) and measurement point 'e' the lowest temperature at its peak (135.18 °C) compared to the remaining measurement points. The slightly higher peak value of the temperature profiles in case of MSS compared to PESS0 can be caused by the spatial positioning of the scanning patterns in the weldMARK 3 software. The reason is that the two scanning patterns can be offset with respect to the defined measuring points in Works software and the higher temperature is detected if the scanning paths of the laser beam are closer to the measuring points. It is worth noting that the temperature detected by the infrared camera is much lower than the melting temperature of the powder. There are several reasons that can explain this temperature difference.

- The observed outcome of processed powder layer was only slightly sintered. This binding mechanism is called solid-state sintering where the target temperature is set between the melting point (M_p) of the material and $M_\mathrm{p}/2$ (Fina et al., 2018). The amount of laser energy employed during the sintering process was below the threshold required to achieve complete sintering. Complete sintering of the powder layer without preheating would have led to the greater thermal stress and significant deformation of the powder

layers (Yan et al., 2021), which in turn would have led to difficulties in estimating the density of the powder layers.

- In the infrared camera settings, the emissivity factor of the powder is set before starting the measurements and remains constant (0.95) during the measurements without the possibility of readjustment. A significant change of the emissivity during the phase transition between solid and molten powder also leads to inaccurate temperature measurements (Laumer et al., 2014). The use of multi-wavelength pyrometer could measure emissivity in real time and confirm the correct temperature measurement conditions.
- During the sintering process, heat can dissipate from the powder layer, especially if it is not well-insulated (experimental conditions: a 400 µm layer was applied to the building platform made up of steel). The heat dissipation to the building platform can lead to lower recorded temperatures than expected, even though the powder layer is sintered.

Notably, the irradiation time of the powder layer using MSS and PESS0 was approximately the same and was 2.88 s and 2.90 s, respectively. When using PESS0, the irradiation time can be fine-tuned for each pixel by adjusting the parameters $t_{\max \mathrm{PE}}$ and $t_{\min \mathrm{PE}}$.

Figure 5 shows the results of sintered layers after irradiation with two scanning strategies. Based on the quantitative analysis, it can be deduced that the MSS approach resulted in 97.86 ± 1.06 % of sintered layer density (percentage of black pixels within sintered layer). In turn, the PESS0 strategy yielded a sintered layer density of 98.11 ± 0.26 %. The identical density of the sintered layers also confirms the similarity of the temperature behavior during powder sintering process using MSS and PESS0.

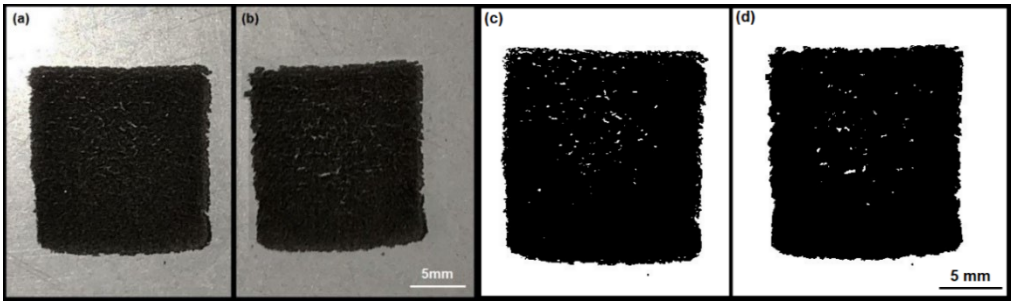

Fig. 5. Sintered single layers; a) applying MSS; b) applying PESS0; c) applying MSS (processed); d) applying PESS0 (processed)

The obtained results allow to conclude that the PESS can also be used in the PBF-LB/P process for sintering powder layers. Consequently, subsequent studies were conducted to tailor the temperature profiles using the developed scanning strategy.

3.2. Tailoring temperature profiles within single layer

In order to demonstrate the ability of the developed scanning strategy to adjust the temperature profiles within a single layer, PESS1 and PESS2 were implemented. Using PESS1 and PESS2 (cf. Fig. 2 and Table 1), the temperature profiles shown in Figure 6 were obtained. Two intensity values of pixels were encoded in PESS1. The first half of the scanning strategy contained black pixels (intensity value - 0), and the second half contained gray pixels (intensity value - 48). The irradiation time of PESS1 (2.36 s) decreased compared to PESS0 (2.90 s) because the irradiation of gray pixels is faster, thus confirming the decrease in delivered energy density. In the upper part of the sintered layer (measuring points T_a, T_b), the maximum temperature reached is 141.52 °C and 135.11 °C, respectively (Fig. 6, a). In the middle of the sintered layer (measuring point T_c), in the transition zone of black pixels to gray pixels of the scanning strategy, the measured temperature peak is recorded at

126.21 °C. At the lower part of the sintered layer (measuring points T_d, T_e) the maximum temperatures of the profiles reached 120.49 °C and 117.40 °C, respectively. The resulting temperature profiles exhibit a strong correlation with the appearance of the sintered single layer as depicted in Figure 6 (a). It can be observed that in the upper region of the layer, a higher amount of thermal energy was imparted to the powder particles, resulting in enhanced particle bonding and the manifestation of a darker coloration within the powder layer. While, the lower region of the powder layer experienced relatively weaker sintering, leading to a lighter coloration of the powder layer.

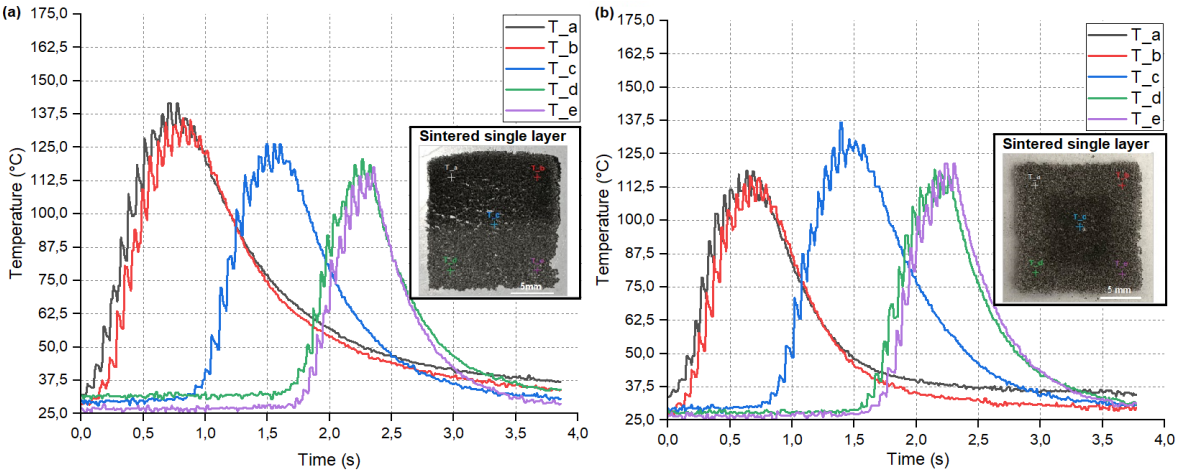

Fig. 6. Resulted temperature profiles of different PESS; a) PESS1 (cf. Fig. 2, (c) and Table 1); b) PESS2 (cf. Fig. 2, (d) and Table 1)

Similar to the PESS1 scanning strategy, the development of PESS2 aimed to showcase the capability of the newly devised scanning approach in generating more intricate temperature profiles. In the middle region of the PESS2, black pixels (intensity value - 0) are present, while the lateral areas consist of gray pixels (intensity value - 48). The sintered layer's central area (measuring point T_c), exhibited the highest temperature peak of 137.48 °C, as depicted in Figure 6 (b). In contrast, the side areas (measuring points T_a, T_b, T_d, T_e) displayed maximum temperature values ranging from 116.60 °C to 121.39 °C in the temperature profiles. Furthermore, Figure 6 (b) visually indicates the resemblance between the appearance of the sintered layer and the applied PESS2.

Conclusion

The high absorptivity of certain polymer powders can result in enhanced heat accumulation and potential thermal damage, especially at the surface of the powder bed. Excessive localized heating can lead to melting, degradation, or undesirable chemical reactions within the polymer material, compromising the structural integrity and overall quality of the fabricated parts. The investigated scanning strategy enables the creation and tailoring of nearly arbitrary temperature profiles within a single layer during the PBF-LB/P process. This scanning approach serves as an effective means of controlling energy density to prevent heat accumulation during powder layer sintering. Consequently, it provides an additional degree of freedom for regulating energy density within a single layer, which proves crucial, particularly when processing highly absorptive polymers that are susceptible to infrared radiation and prone to overheating.

Furthermore, the pixel-encoded scanning strategy exhibits potential for application in the PBF-LB/P process for fabricating multi-material parts. This stems from the fact that different polymer powders may possess

distinct sintering points, necessitating precise adjustment of the applied energy density within each layer to achieve sufficient sintering for each individual powder. By offering the capability to precisely control energy density, the scanning strategy can facilitate the successful integration of multiple polymer powders, thereby enabling the generation of multi-material parts with desirable characteristics.

Acknowledgements

The authors gratefully acknowledge funding of the Collaborative Research Center 814 (CRC 814), subproject B6, by the German Research Foundation (DFG) – project number 61375930 – and support by the Erlangen Graduate School in Advanced Optical Technologies (SAOT) by the Bavarian State Ministry for Science and Art.

References

Ahmadi Dastjerdi, A., Movahhedy, M. R., & Akbari, J. (2017). Optimization of process parameters for reducing warpage in selected laser sintering of polymer parts. *Additive Manufacturing*, *18*(2010), 285–294. https://doi.org/10.1016/j.addma.2017.10.018

Athreya, S. R., Kalaitzidou, K., & Das, S. (2011a). Mechanical and microstructural properties of Nylon-12/carbon black composites: Selective laser sintering versus melt compounding and injection molding. *Composites Science and Technology*, *71*(4), 506–510. https://doi.org/https://doi.org/10.1016/j.compscitech.2010.12.028

Athreya, S. R., Kalaitzidou, K., & Das, S. (2010). Processing and characterization of a carbon black-filled electrically conductive Nylon-12 nanocomposite produced by selective laser sintering. *Materials Science and Engineering A*, *527*(10–11), 2637–2642. https://doi.org/10.1016/j.msea.2009.12.028

Athreya, S. R., Kalaitzidou, K., & Das, S. (2011b). Mechanical and microstructural properties of Nylon-12/carbon black composites: Selective laser sintering versus melt compounding and injection molding. *Composites Science and Technology*, *71*(4), 506–510. https://doi.org/10.1016/j.compscitech.2010.12.028

Caulfield, B., McHugh, P. E., & Lohfeld, S. (2007). Dependence of mechanical properties of polyamide components on build parameters in the SLS process. *Journal of Materials Processing Technology*, *182*(1), 477–488. https://doi.org/https://doi.org/10.1016/j.jmatprotec.2006.09.007

Diegel, O., Nordin, A., & Motte, D. (2019). *Additive Manufacturing Technologies*. 19–39. https://doi.org/10.1007/978-981-13-8281-9_2

Fantino, E., Roppolo, I., Zhang, D., Xiao, J., Chiappone, A., Castellino, M., Guo, Q., Pirri, C. F., & Yang, J. (2018). 3D Printing/Interfacial Polymerization Coupling for the Fabrication of Conductive Hydrogel. *Macromolecular Materials and Engineering*, *303*(4), 1700356. https://doi.org/https://doi.org/10.1002/mame.201700356

Fina, F., Gaisford, S., & Basit, A. W. (2018). Powder bed fusion: The working process, current applications and opportunities. *AAPS Advances in the Pharmaceutical Sciences Series*, *31*, 81–105. https://doi.org/10.1007/978-3-319-90755-0_5

Han, W., Kong, L., & Xu, M. (2022). Advances in selective laser sintering of polymers. *International Journal of Extreme Manufacturing*, *4*(4). https://doi.org/10.1088/2631-7990/ac9096

Hawkins, W. L., et al. (1960). *Proc. 4th Conf. on Carbon. Rubber Age, 88(2), 279.*

Hawkins, W. L., et al. (1963). Synergistic antioxidant combinations. Carbon black substitutes. Journal of Polymer Science Part A: General Papers, 1(11), 3489-3497. *Journal of Polymer Science Part A: General Papers*.

Ho, H. C. H., Gibson, I., & Cheung, W. L. (1999). Effects of energy density on morphology and properties of selective laser sintered polycarbonate. *Journal of Materials Processing Technology*, *89–90*, 204–210. https://doi.org/https://doi.org/10.1016/S0924-0136(99)00007-2

John D williams, & Carl R. Deckard. (1998). Advances in modelingthe effects of selectedparameters on theSLS process. *Rapid Prototyping Journal*, *4*(2), 90–100.

Kruth, J. P., Wang, X., Laoui, T., & Froyen, L. (2003). Lasers and materials in selective laser sintering. *Assembly Automation*, *23*(4), 357–

371. https://doi.org/10.1108/01445150310698652

Laumer, T., Stichel, T., Amend, P., Roth, S., & Schmidt, M. (2014). Analysis of temperature gradients during simultaneous laser beam melting of polymers. *Physics Procedia*, *56*(C), 167–175. https://doi.org/10.1016/j.phpro.2014.08.159

Leary, M. (2020). Chapter 11 - Powder bed fusion. In M. B. T.-D. for A. M. Leary (Hrsg.), *Additive Manufacturing Materials and Technologies* (S. 295–319). Elsevier. https://doi.org/https://doi.org/10.1016/B978-0-12-816721-2.00011-7

Li, Z., Wang, Z., Gan, X., Fu, D., Fei, G., & Xia, H. (2017). Selective Laser Sintering 3D Printing: A Way to Construct 3D Electrically Conductive Segregated Network in Polymer Matrix. *Macromolecular Materials and Engineering*, *302*(11), 1700211. https://doi.org/https://doi.org/10.1002/mame.201700211

Manshoori Yeganeh, A., Movahhedy, M. R., & Khodaygan, S. (2019). An efficient scanning algorithm for improving accuracy based on minimising part warping in selected laser sintering process. *Virtual and Physical Prototyping*, *14*(1), 59–78. https://doi.org/10.1080/17452759.2018.1511738

Papadopulos, F., Spinelli, M., Valente, S., Foroni, L., Orrico, C., Alviano, F., & Pasquinelli, G. (2009). Common Tasks in Microscopic and Ultrastructural Image Analysis Using ImageJ. *Ultrastructural pathology*, *31*, 401–407. https://doi.org/10.1080/01913120701719189

RaylaseAG. (2014). *weldMARK 3 - Remote Interface*. https://www.raylase.de/en/products/software-weldmark-3.html

Rong-ji, W., Xin-hua, L., Qing-ding, W., & Lingling, W. (2009). Optimizing process parameters for selective laser sintering based on neural network and genetic algorithm. *The International Journal of Advanced Manufacturing Technology*, *42*, 1035–1042.

Shen, F., Zhu, W., Zhou, K., & Ke, L. L. (2021). Modeling the temperature, crystallization, and residual stress for selective laser sintering of polymeric powder. *Acta Mechanica*, *232*(9), 3635–3653. https://doi.org/10.1007/s00707-021-03020-6

Shi, Y., Wang, Y., Chen, J., & Huang, S. (2008). Experimental investigation into the selective laser sintering of high-impact polystyrene. *Journal of Applied Polymer Science*, *108*(1), 535–540. https://doi.org/https://doi.org/10.1002/app.27686

Singh, S., Sharma, V., & Anish, S. (2012). Optimization and Analysis of Shrinkage in Selective Laser Sintered Polyamide Parts. *Materials and Manufacturing Processes*, *27*, 707–714. https://doi.org/10.1080/10426914.2011.593247

Stichel, T., Brachmann, C., Raths, M., Dechet, M. A., Schmidt, J., Peukert, W., Frick, T., & Roth, S. (2020). Electrophotographic Multilayer Powder Pattern Deposition for Additive Manufacturing. *Jom*, *72*(3), 1366–1375. https://doi.org/10.1007/s11837-019-03965-z

Van Hooreweder, B., Moens, D., Boonen, R., Kruth, J.-P., & Sas, P. (2013). On the difference in material structure and fatigue properties of nylon specimens produced by injection molding and selective laser sintering. *Polymer Testing*, *32*(5), 972–981. https://doi.org/https://doi.org/10.1016/j.polymertesting.2013.04.014

Wagner, T., Höfer, T., Knies, S., & Eyerer, P. (2004). *Laser Sintering of High Temperature Resistant Polymers with Carbon Black Additives*. *19*(4), 395–401. https://doi.org/doi:10.3139/217.1846

Wegner, A. (2015). Theorie über die Fortführung von Aufschmezvorgängen als Grundvoraussetzung für eine robuste Prozessführung beim Laser-Sintern von Thermoplasten. *Dissertation*, *1*.

Yan, C., Hao, L., Xu, L., & Shi, Y. (2011). Preparation, characterisation and processing of carbon fibre/polyamide-12 composites for selective laser sintering. *Composites Science and Technology*, *71*(16), 1834–1841. https://doi.org/https://doi.org/10.1016/j.compscitech.2011.08.013

Yan, C., Li, Z., Wei, Q., Shi, Y., Wen, S. (2021). Selective Laser Sintering Additive Manufacturing Technology. *A volume in 3D Printing Technology Series. https://doi.org/10.1016/C2018-0-01960-X*

Zhu, W., Yan, C., Shi, Y., Wen, S., Liu, J., & Shi, Y. (2015). Investigation into mechanical and microstructural properties of polypropylene manufactured by selective laser sintering in comparison with injection molding counterparts. *Materials & Design*, *82*, 37–45. https://doi.org/https://doi.org/10.1016/j.matdes.2015.05.043